Colloids and Surfaces B: Biointerfaces 166 (2018) 323–329

Contents lists available at ScienceDirect

Colloids and Surfaces B: Biointerfaces

journal homepage: www.elsevier.com/locate/colsurfb

Exploring the influence of Diels–Alder linker length on photothermal molecule release from gold nanorods

Claudia Vetterlein[a,b], Rodrigo Vásquez[a,b,c], Karen Bolaños[b,c], Gerardo A. Acosta[d,e], Fanny Guzman[f], Fernando Albericio[d,e,g], Freddy Celis[h], Marcelo Campos[i], Marcelo J. Kogan[a,b,*], Eyleen Araya[c,*]

[a] Departamento de Química Farmacológica y Toxicológica, Facultad de Ciencias Químicas y Farmacéuticas, Universidad de Chile, Santos Dumont 964, Independencia, Santiago, Chile
[b] Advanced Center for Chronic Diseases (ACCDiS), Santos Dumont 964, Independencia, Santiago, Chile
[c] Departamento de Ciencias Quimicas, Facultad de Ciencias Exactas, Universidad Andres Bello, Av. Republica 275, Santiago, Chile
[d] CIBER-BBN, Networking Centre on Bioengineering, Biomaterials and Nanomedicine, Barcelona Scientific Park, Baldiri Reixac 10, Barcelona 08028, Spain
[e] Department of Organic Chemistry, University of Barcelona, Martí i Franquès 1-11, Barcelona 08028, Spain
[f] Núcleo de Biotecnología Curauma, Pontificia Universidad Católica de Valparaiso, Av Universidad 330 Curauma, Valparaiso, Chile
[g] School of Chemistry & Physics, University of Kwazulu-Natal, Durban 4001, South Africa
[h] Departamento de Química y Centro de Estudios Avanzados, Universidad de Playa Ancha, Casilla 34-V, Valparaíso, Chile
[i] Department of Chemistry, Faculty of Sciences, University of Chile, POBox 653, Santiago, Chile

ARTICLE INFO

Article history:
Received 18 October 2017
Received in revised form 1 February 2018
Accepted 17 March 2018
Available online 19 March 2018

Keywords:
Controlled release
Photothermal effect
Fluorescence
Spatial temporal release

ABSTRACT

We studied the photothermal release of carboxyfluorescein (CF) linked to the gold surface of gold nanorods (GNRs) by two Diels–Alder adducts of different lengths (n = 4 and n = 9). The functionalized GNRs were irradiated with infrared light to produce photothermal release of CF by a retro-Diels–Alder reaction. The adducts were chemisorbed on the GNRs and the functionalized nanoparticles were characterized by UV–vis, DLS, zeta potential and Raman and surface-enhanced Raman spectroscopy (SERS). On the basis of the degree of nanoparticle functionalization and the SERS results, we inferred the orientation of CF on the surface of the gold nanoparticle. Moreover, we determined the photothermal release profiles of CF from the gold surface by laser irradiation. The release was faster for the longer linker (n = 9). SERS revealed that, for the shorter linker (n = 4), molecules are oriented perpendicularly with respect to the gold surface, thereby maintaining the CF far from the surface. In contrast, the longer linker was observed to be tilted, thus maintaining CF close to the gold surface and therefore potentially favoring the photothermal transfer of energy. These results are relevant for the future development of the spatial and temporal controlled release of drugs by means of gold nanoparticles.

1. Introduction

Spatial and temporal controlled release systems that respond to external *stimuli* have multiple medical applications, such as for drug delivery [1–17]. Nanoparticles formed by noble metals can absorb photons, thus dissipating the energy absorbed and producing local heat as a result of the surface plasmon resonant effect (SPR) [18]. This effect occurs in gold nanorods [GNRs] with an aspect ratio (length/width) at wavelengths in the near infrared region from 700 to 1300 nm. This nanomaterial is especially suited for biomedical applications because tissues and cells have low absorption coefficients in this region [19]. One interesting application of GNRs is traditional hyperthermia for the treatment of cancer, where the region of the body containing the tumor is heated to ~40–45 °C—several degrees above physiological temperature (37 °C) [20]. In the case of GNRs, the heat is generated externally using a laser. The photothermal traits may render some cancer cells more sensitive to heat [21]. However, here we sought to use the laser to achieve the photothermal release of a molecule.

Bakhtiari et al. [22] developed an efficient method based on a photothermal effect to release 5[6]-carboxyfluorescein (CF) from spherical gold nanoparticles and silica-gold core-shells. Gold sur-

* Corresponding authors at: Departamento de Química Farmacológica y Toxicológica, Facultad de Ciencias Químicas y Farmacéuticas, Universidad de Chile, Santos Dumont 964, Independencia, Santiago, Chile and Departamento de Ciencias Quimicas, Facultad de Ciencias Exactas, Universidad Andres Bello, Av. Republica 275, Santiago, Chile.
E-mail addresses: mkogan@ciq.uchile.cl (M.J. Kogan), eyleen.araya@unab.cl (E. Araya).

https://doi.org/10.1016/j.colsurfb.2018.03.021
0927-7765/

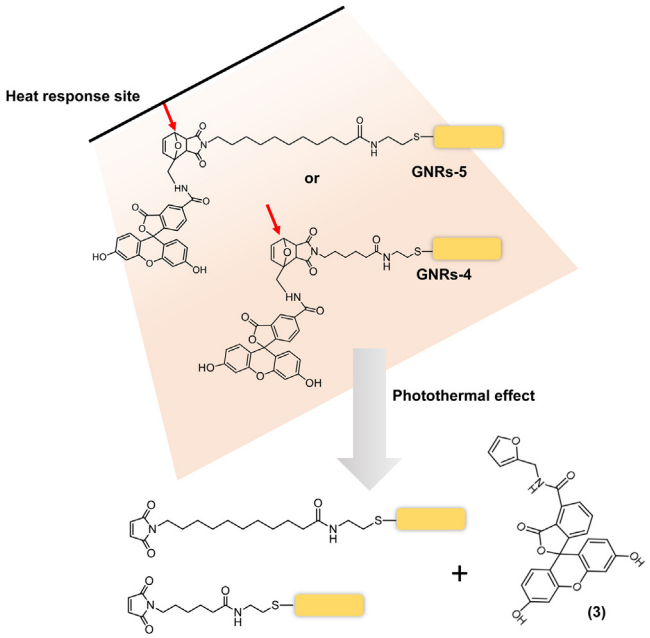

Fig. 1. Scheme of the photothermal release of **(3)** from GNRs-4 and GNRs-5 produced by a retro-Diels–Alder reaction after irradiation with a laser. The cleavage sites are shown by red arrows. (For interpretation of the references to colour in this figure legend, the reader is referred to the web version of this article.)

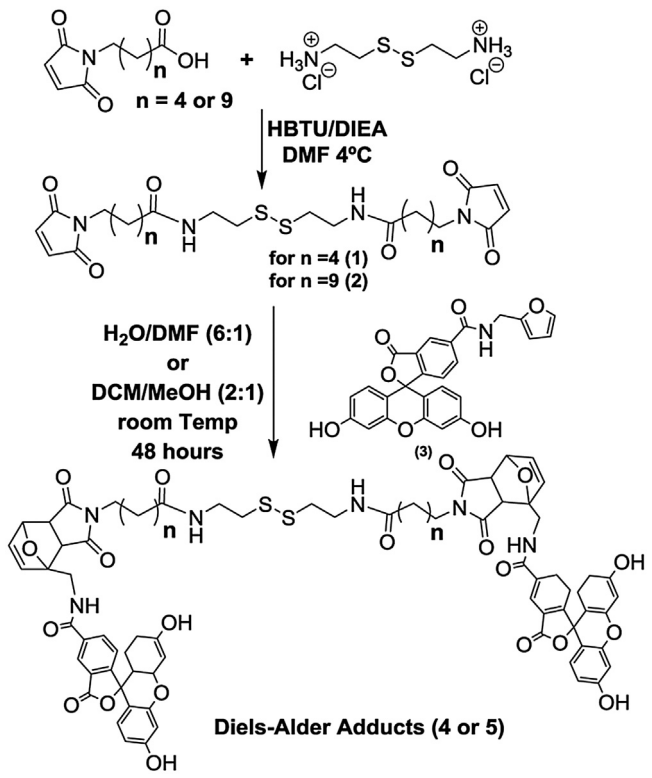

Fig. 2. Scheme of the synthesis of **(4)** with 6-maleimido hexanoic acid and **(5)** with 11-maleimido undecanoic acid.

faces were functionalized with a bifunctional linker that had CF bound to a Diels–Alder adduct at one and a sulfur at the other end, which allowed chemisorption to the gold surface. After irradiation of the functionalized gold nanoparticles, the Diels–Alder adduct is degraded by means of a retro-Diels–Alder reaction, thus releasing CF [22] by the photothermal effect. Furthermore, Yamashita et al. [23] reported the controlled release of polyethylene glycol (PEG) molecules from GNRs by a retro-Diels–Alder reaction produced by the photothermal effect. Recently, Asadirad et al. [24] demonstrated the photothermal release of dithienylethene chromophores from the surface of nanoparticles.

In view of the increased potential applications of gold nanoparticles for the spatial and temporal controlled release of drugs, it is important to explore a range of nanomaterials and linkers of distinct length in order to determine their influence on the photothermal release of the drug. A highly relevant aspect is to determine the degree of functionalization and the orientation of the molecules on the surface of the gold nanoparticle, as functionalization influences the effectivity of the photothermal process [25]. Thus, it is critical to evaluate the effectiveness of drug release from the surface of gold nanoparticles are bound to the linker and irradiated.

Here we functionalized GNRs with two bifunctional linkers (n = 4 and n = 9) of different length that contain a sulfur molecule at one end to allow chemisorption to the gold surface and a CF Diels–Alder adduct at the other, obtaining the GNRs-4 and GNRs-5, respectively (Fig. 1). We examined the effect of linker length on the photothermal release of the molecule by applying near infrared irradiation with a laser that favors the retro-Diels–Alder reaction.

Two linkers [n = 4 and n = 9] were synthesized by Diels–Alder cycloaddition reaction with **(3)** (see Fig. 2), and GNRs were functionalized with the linkers, thus obtaining GNRs-4 and GNRs-5, respectively (Fig. 1). The functionalized nanoparticles were then characterized by UV–vis-NIR, Scanning Transmission Electron Microscopy (STEM), Dynamic Light Scattering (DLS) and zeta potential. In order to obtain information about the orientation of the CF molecules on the gold surface, we registered surface-enhanced Raman spectra (SERS). The release of **(3)** was evaluated by irradiation with an 808 nm continuous laser (Fig. 1).

2. Experimental

2.1. Synthesis of the dienophyles N,N-di-6-maleimide-hexanoyl cystamine (1) and N,N-di-11-maleimide-undecanoyl cystamine (2)

In a round-bottomed flask, 556 mg of 6-maleimidehexanoic acid (Sigma, ≥90% purity) and 273 mg of 98% cystamine chlorohydrate (Sigma, ≥98.0% purity) in 3 mL of anhydrous *N,N*-dimethylformamide (DMF) were dissolved. The mixture was cooled to 4 °C and maintained under magnetic stirring. Next, 917 mg of *N*-[(1H −benzotriazol-1-yl)-(dimethylamino)methylene]-N −methylmethanaminium hexafluorophosphate *N*-oxide (HBTU, Merck, ≥ 99.0% purity) and 0.5 mL of *N,N*-Diisopropylethylamine (DIEA) (Merck, ≥98.0% purity) were added to the samples. The reaction was kept at room temperature for 72 h under magnetic stirring. The reaction was stopped by the addition of cold water, obtaining a solid, which was filtered. The solid was then suspended in K_2CO_3, and compound **(1)** (Fig. 2) was extracted in CH_2Cl_2. The organic phase was dried with anhydrous $MgSO_4$. The solvent was removed under vacuum. The product (95% purity) was characterized by EI-MS (LC MS 2020 Liquid Chromatograph Shimadzu) and by ^1H and ^{13}C NMR (Bruker AVANCE III HD de 400 MHz, smartProbe of 36 shims 5 mm H1/BB). (Supporting information, S1)

The dienophyle **(2)** (Fig. 2) was synthesized following the same procedure and using 11-maleimide undecanoic acid (Supporting information, S1).

2.2. Synthesis of the diene (3)

5[6]-Carboxyfluorescein (0.376 g) (Merck, ≥96.0% purity), HBTU (0.379 g) and DIEA (335 μL) were stirred in 3 mL of DMF for 15 min at 0 °C. 2-aminomethylfurane (90 μL) (Merck ≥ 99.0% purity) was then added to the mixture, which was stirred at room temperature for 12 h. Finally, the solvent was evaporated, and the residue was purified by chromatography through silica-gel using CH_2Cl_2/CH_3OH [10:1]. The final product (98% purity) was characterized by EI-MS (Supporting information, S2).

2.3. Synthesis of the Diels–Alder adduct **(4)**

A mixture of 100 mg of (**3**) with 59.3 mg of **(1)** was dissolved in 500 μL of DMF in a dark flask, and 3 mL of water was then added. The reaction was incubated at room temperature under magnetic stirring for 48 h. The solid formed was filtered and lyophilized. The final product (97% purity) was characterized by EI-MS (Supporting information, S3).

2.4. Synthesis of the Diels–Alder adduct **(5)**

In a tube, 12.6 mg of **(3)** was dissolved in 3 mL of CH_2Cl_2/CH_3OH [2:1], and then 6.3 mg of **(2)** was added. The reaction was incubated at 25 °C overnight with magnetic stirring. The solvent was evaporated under vacuum. The final product (97% purity) was characterized by EI-MS (Supporting information, S3).

2.5. Synthesis of GNRs

In the first step, a seed solution of gold nanoparticles was prepared. In a flask, cold-prepared sodium borohydride (600 μL, 0.01 M) was added to 250 μL of $HAuCl_4$ in 9.75 mL of 0.1 M cetyltrimethylammonium bromide (CTAB) under vigorous magnetic stirring. The seeds solution was kept at 27 °C for 2 h before use. Next, 55 μL of 0.1 M ascorbic acid [Sigma Chemical Co., St. Louis, MO, USA] was added to a growth solution containing 75 μL of 0.01 M $AgNO_3$ [Sigma Chemical Co., St. Louis, MO, USA], 9.5 mL of 0.1 M CTAB and 500 μL of 0.01 M $HAuCl_4$. Then, 250 μL of 0.1 M HCl and 12 μL of the previously prepared seed solution were added. The solution was incubated for 10 min at 27 °C before centrifugation at 7,030x*g* for 15 min. After centrifugation, the supernatant was removed, and the pellet was resuspended in Milli-Q water.

2.6. Obtention of GNRs-4 and GNRs-5

4 mL of GNRs-CTAB were centrifuged at 7,030x*g* for 60 min. The supernatant was discarded, and the pellet was resuspended in 4 mL of Milli-Q water. Next, a solution of **(4)** or **(5)** (1 mg/mL, in DMF) was added to the resuspended GNRs, and the mixture was stirred magnetically overnight. The functionalized gold nanorods were centrifuged at 7,030x*g* for 60 min. The supernatant was then removed, and the pellet was resuspended in 5 mL of Milli-Q water.

2.7. Characterization of GNRs

The nanoparticles were characterized by UV–vis-NIR, DLS, Zeta potential and STEM.

UV–vis-NIR absorption spectra were recorded at 25 °C using a Perkin Elmer Lambda 25 spectrophotometer.

DLS analyses were performed at 25 °C by using a Malvern Zetasizer Nano ZS (Malvern Instruments) operating at a light source wavelength of 532 nm and with a fixed scattering angle of 90°. Measurements were made by placing 1 mL of the colloidal sample in a cell with an optical path of 1 cm. To determine the size distribution of the samples, the results were analyzed from the intensity distribution values using the cumulant method.

The zeta potential (Zeta sizer 3000, Malvern Instruments, U.K.) measurements of nanoparticles consisted of five repeats of each GNR solution. Since the zeta potential measurements were performed in an aqueous solution, the Smolochowski approximation was used to calculate them from the electrophoretic mobility measured. The electrophoretic determinations of zeta potential are most commonly performed in aqueous media and a moderate electrolyte concentration.

GNRs were observed using a scanning electron microscope with electronic transmission module [STEM] FEI Inspect F50 (STEM conditions: HV: 30000KV, Mag: 500000, HFW: 597 nm, WD: 4.3 mm, Spot:3.0). The specimens for electron microscopy observation were prepared by dropping GNRs onto Formvar carbon-coated copper microgrids [Ted Pella, Inc. Redding, CA, USA] and allowing them to dry.

2.8. Determination of the number of molecules of (4) and (5) per gold nanorod

Gold was quantified by inductively coupled plasma optical emission spectrometry (ICP-OES). Briefly, a 50-μL sample was digested with 1 mL of 60% HNO_3, 500 μL of 37% HCl and 500 μL of 30% H_2O_2 at 90 °C for 24 h. The digested samples were made up to a volume of 50 mL with 200-ppm thiourea in 1% HCl before analysis by ICP-OES (Perkin Elmer Optima 3200 RL instrument). The gold content was determined from plotting the calibration curve of the standard.

On the basis of the gold concentration (CAu) data and knowledge of the length and width averages of the GNRs (both determined by STEM), the concentration (nanomolar) of GNRs was determined as follows:

$$\text{ConcentrationofGNRs} = 4 \times \text{CAu}/\rho\text{Au} \times \pi \times \text{W} \times 2\text{L}$$

where ρAu is the density of gold atoms in the bulk [59 atoms/nm^3], CAu is the gold concentration determined by gold neutron activation, and L and W are the length and width of GNRs, respectively, determined by STEM.

The number of molecules of **(4)** or **(5)** per GNR was estimated by measuring fluorescence after the centrifugation of the GNRs at 16,560×*g* for 30 min. Under these conditions, the GNRs-4 and GNRs-5 sedimented out and the excess of unbound molecules of **(4)** and **(5)** present in the supernatant was determined by fluorescence in triplicate in three separate analyses.

2.8.1. Stability of GNRs-4 and GNRs-5

The stability of GNRs-4 and GNRs-5 was evaluated by means of UV–vis-NIR, DLS after storage of the samples for 7 days at room temperature.

2.8.2. Raman and surface enhanced Raman scattering measurements

The Raman and SERS measurements were performed using a Renishaw micro-Raman RM 1000 spectrometer, equipped with laser lines of 514, 633 and 785 nm. The spectrometer was coupled to a Leica microscope DMLM and an electrically cooled CCD camera. The Raman signal was calibrated to the 520 cm^{-1} line of silicon and lens of 50x objetive. The samples were deposited on a thin sheet of gold to remove their intrinsic fluorescence. We used various laser lines to obtain the Raman signals of the molecular systems of interest. The best results were obtained at 785 nm and under particular spectral scanning conditions. That is, the power on the sample was carefully considered and consequently used (0.2 mW), being less than 1% of the total power. Acquisition time was set between 10 and 20 s per accumulation; the average number of accumulations

was 5 with spectral resolution of 4 cm^{-1}. The spectra were recorded between 100 and 1800 cm^{-1}. The Raman spectra were registered for the 4 and 5 samples in the solid state. The SERS spectra of the GNRs-4 and GNRs-5 solids were obtained after evaporating the solvent.

2.9. Determination of the photothermal release of (3) from GNRs-4 and GNRs-5

Aliquots of 500 μL of GNRs-4 and GNRs-5 in a glass tube (6 × 50 mm, Kimax ®, Cat- 45048-650) were irradiated for 25, 50 100, 150 and 180 min with a continuous diode laser (808 nm, 350 mW, spot 1 mm, power technology ® laser model IQ1A350) located 10 cm from the tube. The whole procedure was performed in a dark room in order to protect the system from light. The samples were centrifuged at 16,000x*g* for 15 min. Fluorescence intensity at 518 nm (excitation 495 nm) was measured in the supernatants in a Synergy MX apparatus. EI-MS spectra for (**3**) released after the photothermal treatment were collected.

3. Results and discussion

3.1. Obtention of the bifunctional linkers (n = 4 and n = 9) bound to CF

Diels–Alder adducts between CF and with two linkers of different lengths were synthesized following the scheme described in Fig. 2. The corresponding maleimides (n = 4 or 9, Fig. 2) were incubated with cystamine to form the corresponding dienophiles **(1)** and **(2)** (Fig. 2).

The dienophiles (**1**) and (**2**) were purified by column HPLC and characterized by EI-MS, thus detecting $[M+H]^{+}=539$, $[M+2H/2]^{+1}=270$; $2[M+H]^{+1}=1078$ and $(M+H)^{+}=679$; and $(M+2H/2)^{+1}=340$ and $2(M+H)^{+1}=1358$, respectively. Compounds **(1)** and **(2)** were also characterized by ^{1}H NMR (Supporting information, S1).

Therefore, to obtain the diene (3), CF was incubated with 2-furfurylamine to obtain **(3)**, which was analyzed by HPLC and characterized by EI-MS (Supporting information, S2), detecting the $[M+H]^{+1}=456$.

For the cycloaddition, **(1)** and **(2)** were mixed with **(3)** to form the bifunctional linkers containing the Diels–Alder adducts **(4)** and **(5)** (Fig. 2), which were purified and characterized by HPLC–MS (See Supporting information, S3), detecting $[M+H]^{+1}=1450$; $[M+2H/2]^{+1}=725$, $[M+2H/2]^{+1}=484$ and $[M+2H/2]^{+1}=795$, $[M+3H/3]^{+1}=531$, respectively.

3.2. Functionalization of gold nanorods with the linkers (4) and (5)

GNRs-CTAB were obtained by the seed-mediated method [24]. The aspect ratio (length/width) of the GNRs was found to be centered at 4 (40 × 10 nm, length and width, respectively), as determined by STEM (Fig. 3). The GNRs-CTAB were then mixed with (**4**) or (**5**) and incubated in order to obtain GNRs-4 and GNRs-5, respectively. The chemisorption of the disulfides on the gold surface allowed the formation of Au-S bonds [26,27] to form the functionalized GNRs (GNRs-4 and GNRs-5). The UV–vis-NIR spectra of the conjugates were obtained (Fig. 3), showing the characteristic bands that correspond to the transverse and longitudinal plasmon resonance bands centered at 530 and 800 nm, respectively [26,27]. Typically, the surface modification of GNRs is reflected in a plasmon band shift to longer wavelengths due to the change that occurs in the refractive index and dielectric constant of the medium. The characteristic shift of the surface plasmon resonance band (longitudinal plasmonic band) from 800 to about 850 nm was observed in GNRs-4 and GNRs-5 (Fig. 3). Moreover, a broadening of the longitudinal band (app. 530 nm) attributable to the absorbance of CF was detected. The change occurred within a few minutes, thereby indicating rapid conjugation. In addition, no significant broadening of plasmon resonance was seen after conjugation. The conjugates were also characterized by DLS and zeta potential (Table 1).

The hydrodynamic diameter and the zeta potential of the functionalized GNRs were also determined (Table 1). The functionalization of GNRs-CTAB with (**4**) and (**5**) led to an increase in the hydrodynamic diameter. In the case of GNRs-4, the increase in this parameter was more evident, which could be explained by an aggregation process. The neutral molecules (**4**) and (**5**) allowed the reduction of the zeta potential caused by the replacement of CTAB (positively charged).

To estimate the number of molecules of (**4**) and (**5**) grafted on the nanoparticles after conjugation, the solutions of nanoparticles were centrifuged, and fluorescence was determined in the supernatant. On the basis of the difference between the original concentration obtained by fluorescence quantification (solution before conjugation) and the concentration obtained in the supernatant after the conjugation, and the concentration of GNRs determined by ICP-Mass spectrometry, it is possible to estimate the number of grafted molecules per nanoparticle [28]. In both cases, approximately 20,000 molecules were detected per GNR. Assuming that the gold nanorod has a cylindrical shape and a mean size of 40 × 10 nm (length and width, respectively) and a corresponding area of 12,560 nm^2, we estimated the capping of approximately 1.6 molecules (expressed as CF) per nm^2. This value is lower than that found for alkanethiols forming a self-assembled monolayer (SAM) [3.6 molecules per nm^2]. [29]. The lower degree of functionalization of GNRs for **(4)** and **(5)** with respect to that obtained for alkenethiols that form a SAM can be explained by the steric hindrance produced by CF, which prevents self-assembly, thus reducing the density of molecules per nm^2.

3.3. Exploring the orientation of *(4)* and *(5)* in GNRs-4 and GNRs-5 by Raman spectroscopy

A vibrational analysis using Raman spectroscopy and surface-enhanced Raman scattering (SERS) techniques was performed in order to infer the orientation and organization of **(4)** and **(5)** on the gold surface. SERS allows access to information for fluorescent molecular systems due to the quenching produced by metallic nanoparticles, particularly when working with metallic colloidal solutions [30]. Also, SERS can provide information about the activity of analytes present at very low concentrations, achieving the limits of the single molecule detection [31,32].

The Raman spectra of **(4)** and **(5)** are shown in red in Fig. 4A and B, respectively. The profiles are nearly identical; some of the relative intensity modifications observed are due to conformational changes. In fact, Raman signals in the 950–1150 cm^{-1} spectral region, corresponding to vibrational modes belonging to the aliphatic chains [stretching CC modes, νCC], are mostly modified [33,34]. On the other hand, the relative intensity of the band at about 1650 cm^{-1}, attributed to the carbonyl group, also changed, which is interpreted as conformational modifications in this fragment. This vibration can provide information on the fragment on the aliphatic chain as the inter ring moiety of the fluorophore. The band at about 1770 cm^{-1} in both spectra was assigned to a νCO vibration of the fluorophore [35].

The SERS spectra of functionalized GNRs-4 and GNRs-5 are shown in black in Fig. 4A and B, respectively. In general, spectral modifications of the bands are expected due to the interaction of the molecules with the metal surface. Frequency shifts and relative intensity modifications can be associated with chemical interac-

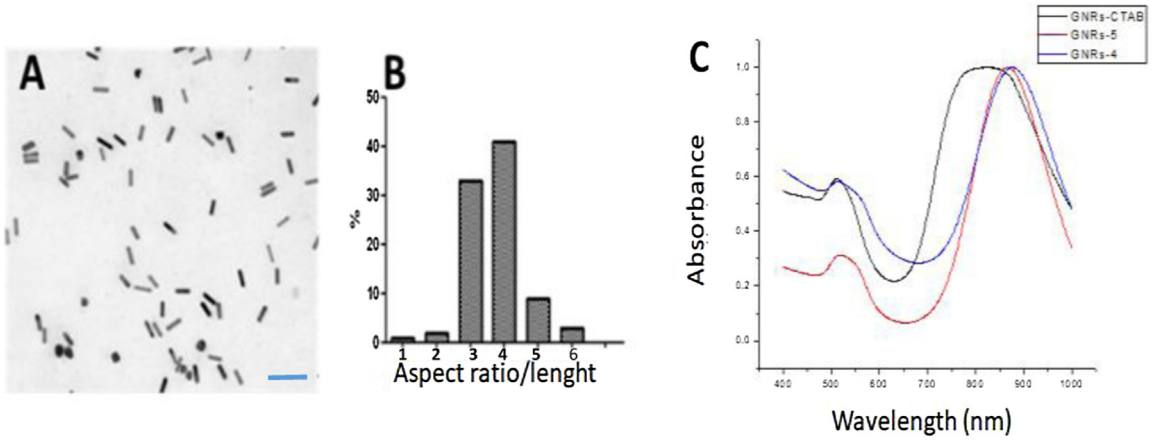

Fig. 3. A] STEM micrograph of GNRs-CTAB (the bar represent 100 nm) B] Histogram aspect ratio considered for 100 particles of GNRs-CTAB. C] UV–vis-NIR spectra of GNRs-CTAB, GNRs-4 and GNRs-5.

Table 1
Characterization of GNRs-CTAB, GNRs-4 and GNRs-5.

Gold Nanoparticle	Average Hydrodynamic Diameter [nm]	Polydispersity Index	Zeta Potential [mV]
GNRs-CTAB	3/70	0.4	+43 ± 3
GNRs-4	17/175	0.4	+6 ± 3
GNRs-5	2/76	0.4	+30 ± 4

tions and with the proximity and/or preferential orientation of the analyte on the metal surface. Any molecular fragment located far from the surface has no SERS signal. In the present case, the spectral profiles differed; frequency shifting, intensity modifications and the appearance or disappearance of bands were observed. As a hypothesis, if the fluorophore is far from the surface, the SERS bands should be absent or weak and the analyte-gold surface interaction should occur through the sulfur atom. Some particular bands were intense, thereby indicating a preferential orientation of the molecules on the surface. In the case of GNRs-4, the carboxyl band of the fluorophore at 1779 cm^{-1} shifted to 1781 cm^{-1} as a result of the metal surface effect, thereby decreasing its relative intensity. The corresponding molecular moiety was far from the surface or the vibrating mode was tilted to the surface.

The strong band at 1340 cm^{-1} belonging to lactone and aromatic esters of the fluorophore was weak in the SERS spectra, thereby suggesting that the fluorophore was far from the metal surface and had no preferential orientation. The same situation and interpretation can be put forward for the aromatic ring band at 1190 cm^{-1} (Fig. 4).

The most significant spectral change was for the strong band at 742 cm^{-1}, which was absent in the SERS spectrum. This band was ascribed to a νC—S mode; this vibration appears in alkyl sulfides as one or more bands. If the corresponding bond is in a plane parallel to the surface, the SERS selection rules indicate that the vibrating mode should not be observed [36,37]. This bond may also be electronically modified because of the eventual gold sulfur interaction. This interaction is verified by the appearance of the band at 280 cm^{-1} in the SERS spectrum. Another νCS band at 642 cm^{-1} showed an increase in relative intensity and a shift to 634 cm^{-1} caused by surface effect, thereby confirming that the interaction involves the CS molecular fragment.

In the case of GNRs-5, the general Raman and SERS spectral profiles differed (Fig. 4). The CO fluorophore band at 1776 cm^{-1} practically disappeared as a result of surface effect. The CO fluorophore bands at 1424 and 1338 cm^{-1} shifted to 1454 and 1326 cm^{-1}, respectively. In the former, a relative increase in intensity was observed, caused by the metal surface effect. However, the opposite was observed for the second band. These spectral changes indicate a weak chemical interaction between the surface and the fluorophore. The low decrease in the relative intensity of the fluorophore ring band at 1190 cm^{-1} indicates that the corresponding molecular fragment of the fluorophore is not far from the surface.

SERS bands between 950 and 1150 cm^{-1}, attributable to the aliphatic chain vibrations, were clearly observed, indicating that these modes vibrated close to the surface. The νCS Raman bands at 742 and 639 cm^{-1} showed an apparent shift to 761 and 647 cm^{-1}, respectively. These bands showed a strong relative intensity in SERS. This spectral behavior indicates that both vibrations are influenced by the metal surface interaction. The SERS band at 761 cm^{-1} was associated with a vibration of the epoxy moiety of the fluorophore. The increase in its relative intensity was due to its proximity to the surface. The νCS band at 647 cm^{-1} displaying medium intensity was influenced by the surface interaction, and the orientation of the corresponding CS bond was probably tilted to the surface.

In conclusion, we propose that molecules **(4)** are oriented perpendicular to the surface of the GNRs and interact through the sulfur atom (Fig. 5). Regarding **(5)**, the results indicate that the whole molecule was tilted on the surface, and the interaction with the surface probably occurs through the sulfur atom, In this case, the fluorophore and the aliphatic moieties were structurally influenced by the surface. The longer hydrocarbon chain in (**5**) conferred flexibility to the system, thus allowing interaction between the fluorophore and the surface.

3.4. Comparison of the photothermal release of (3) from GNRs-4 and GNRs-5

The release of **(3)** was evaluated by fluorescence. The samples were irradiated with a 808 nm laser (350 mW) for 25, 50, 100, 150 and 180 min (Fig. 6). To separate the molecules released, the samples were centrifuged at 16,000xg. The intensity of fluorescence was determined in the supernatants. The values obtained are expressed as percentage of release with respect to the maximum value obtained in the samples of GNRs heated at 90 °C for 30 min [Supporting material, S4].

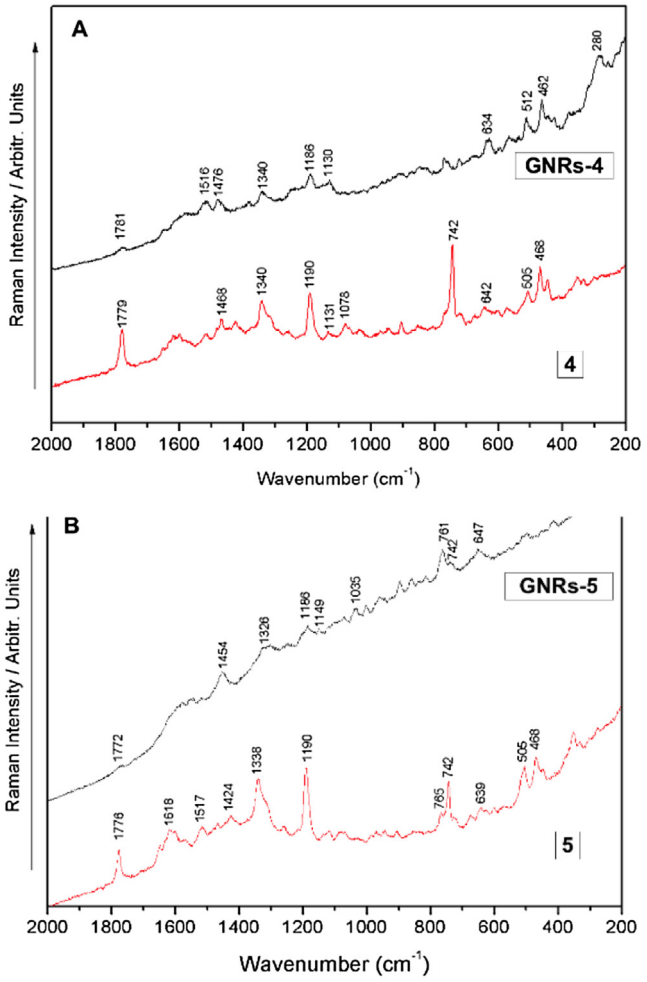

Fig. 4. [A] Raman spectrum of **(4)** (red) and SERS spectrum of GNRs-4 (in black). [B] Raman spectrum of **(5)** (red) and SERS spectrum of GNRs-5 (black), in the solid state. (For interpretation of the references to colour in this figure legend, the reader is referred to the web version of this article.)

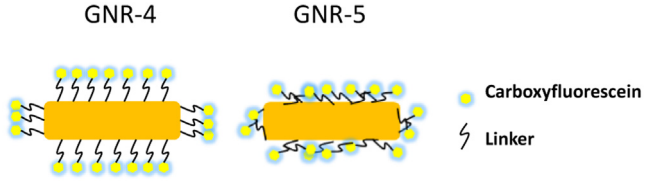

Fig. 5. Hypothetical scheme for the orientation of (**4**) [perpendicular] and (**5**) [titled] on the GNR surface.

The release of **(3)** by heating the solution was faster than that produced by the photothermal effect. Notably, the release profiles of GNRs-4 and GNRs-5 differed. After 3 h of irradiation, the maximum release of **(3)** from both types of GNR was achieved. However, the release of **(3)** for GNRs-5 started after 30 min of irradiation. In contrast, in the case of GNRs-5, the release started at 90 min of irradiation and complete release was achieved at 150 min. In contrast, the complete release of **(3)** from GNRs-4 was observed at 180 min of irradiation. Moreover, in order to detect **(3)** released in the supernatant of the irradiated samples, EI-MS spectra were examined [supporting information, S5]. Additionally, in order to determine whether the (3) remains on the surface of the nanoparticles after irradiation, we compared the SERS signals of the pellets before and after irradiation of the samples. We observed a considerable decrease in the signal intensities of (3). Notably, the typical

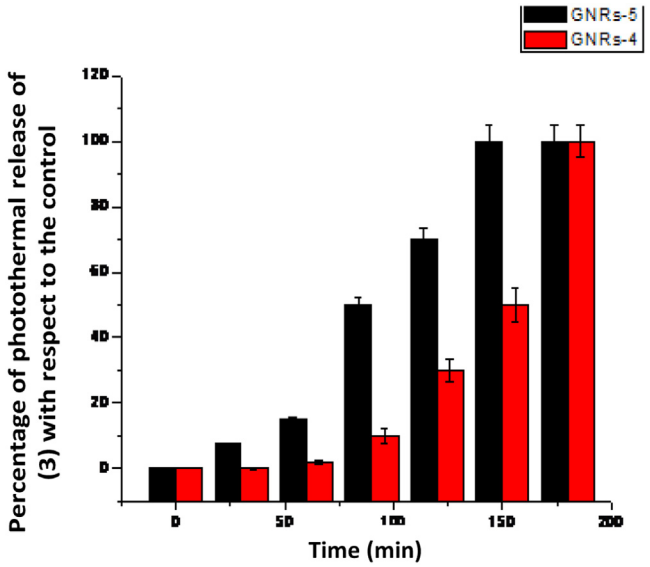

Fig. 6. Release profile of **(3)** after irradiation of GNRs-4 and GNRs-5 with a laser of 808 nm [350 mW]. The samples were centrifuged for 15 min at 16,000×*g*. Fluorescence at 518 nm was determined [excitation at 495 nm]. The percentage of fluorescence is expressed with respect to the release of the molecule after heating at 90 °C [considered as 100%]. The experiments were performed in triplicate.

signal of the fluorophore ring band at 1190 cm^{-1} showed a decrease in intensity after irradiation of GNRs-4 and GNRs-5, which is consistent with its release from the surface after 3 h of irradiation (Supporting information, S6).

Moreover, in order to determine whether irradiation affects the colloidal stability of the samples, UV–vis-NIR spectra and DLS were collected. Small changes in the plasmon bands [Supporting information, S7] and no variation of the hydrodynamic diameters or morphology of the nanoparticles (TEM) were observed (data not shown).

Furthermore, the temperature of GNRs-4 and GNRs-5 was determined after different periods of laser irradiation, thus observing an average temperature of 46 °C and 48 °C, respectively. In order to discard the release occurring by heating the bulk, we heated the GNRs-4 and GNRs-5 solutions at 48 °C for 180 min and no release of (3) was detected.

The orientation of Diels–Alder adducts with respect to the surface is relevant for the transfer of energy produced by the photothermal effect. As discussed previously, the molecules (**3**) in GNRs-5 were titled on the surface of the rods. This titled orientation can favor the approach of the molecule to the surface and can contribute to a better heat transfer from the irradiated GNR to produce the retro-Diels–Alder reaction. Bhana et al. [38] demonstrated that the length of linkers used for photothermal applications is relevant in relation to the release of loaded antitumor drug and the killing of cells through the photothermic effect. However, to the best of our knowledge, no previous study has addressed the effect of linker length on photothermal release and the photothermal cleavage of linkers.

4. Conclusions

GNRs were functionalized with two linkers of different lengths that contain a Diels–Alder adduct to allow the photothermal release of CF. Characterization of the functionalized nanoparticles by various techniques and by Raman spectroscopy and SERS was carried out. These approaches contributed to determining that the orientation of the linker molecules depends on their length. The controlled release of **(3)** after the application of a continuous laser of 808 nm

was demonstrated. The time profile for the release of the fluorescent molecule was dependent on the linker length. Given that the degree of functionalization is not dependent on the length of the linkers used, this distinct behavior regarding photothermal release could be attributed to the orientation of the molecules on the gold surface. Understanding the parameters that influence the photothermal release of biomolecules is highly relevant for future applications of these materials involving the spatial and temporal controlled release of drugs.

Acknowledgments

Fondecyt 11130494, Fondap 15130011, DI 1309/16R.

Appendix A. Supplementary data

Supplementary data associated with this article can be found, in the online version, at https://doi.org/10.1016/j.colsurfb.2018.03.021.

References

[1] S. Hernot, A.L. Klibanov, Adv. Drug Deliv. Rev. 60 (2008) 1153.
[2] S.L. Huang, Adv. Drug Deliv. Rev. 60 (2008) 1167.
[3] X. Guo, F.C. Szoka, Acc. Chem. Res. 36 (2003) 335.
[4] G.F. Walker, C. Fella, J. Pelisek, J. Fahrmeir, S. Boeckle, M. Ogris, E. Wagner, Mol. Ther. 11 (2005) 418.
[5] S. Freiberg, X.X. Zhu, Int. J. Pharm. 282 (2004) 1.
[6] V.P.J. Torchilin, Controll. Release 73 (2001) 137.
[7] Y. Bae, S. Fukushima, A. Harada, K. Kataoka, Angew. Chem. Int. Ed. 42 (2003) 4640.
[8] E.S. Lee, K.T. Oh, D. Kim, Y.S. Youn, Y.H.J. Bae, Controll. Release 123 (2007) 19.
[9] F. Meng, Z. Zhong, J. Feijen, Biomacromolecules 10 (2009) 197.
[10] O. Soga, C.F. Van Nostrum, M. Fens, C.J.F. Rijcken, R.M. Schiff;;elers, G. Storm, W.E.J. Hennink, Controll. Release 103 (2005) 341.
[11] C.S. Brazel, Pharm. Res. 10 (2009) 644.
[12] T.Y. Liu, S.-H. Hu, D.-M. Liu, S.-Y. Chen, I.-W. Chen, Nanotoday 4 (2009) 52.
[13] M.B. Cortie, D. Pissuwan, T. Niidome, J. Controll. Release 149 (2011) 65.
[14] B.P. Timko, T. Dvir, D.S. Kohane, Adv. Mater. 22 (2010) 4925.
[15] G. Han P. Ghosh, M. De, Kim, V.M. Rotello, Adv. Drug Deliv. Rev. 60 (2008) 1307.
[16] R.A. Sperling, P.R. Gil, F. Zhang, M. Zanella, W.J. Parak, Chem. Soc. Rev. 37 (2008) 1896.
[17] D.A. Giljohann, D.S. Seferos, W.L. Daniel, M.D. Massich, P.C. Patel, C.A. Mirkin, Angew. Chem. Int. Ed. 49 (2010) 3280.
[18] M.A. El-Sayed, X.H. Huang, S. Neretina, Adv. Mater. 21 (2009) 4880.
[19] R. Weissleder, Nat. Biotechnol. 19 (2001) 316.
[20] S.B. Field, N.M. Bleehen, Cancer Treat. Rev. 6 (1979) 63.
[21] N.S. Abadeer, C.J. Murphy, J. Phys. Chem. C 120 (2016) 4691.
[22] A.B. Bakhtiari, D. Hsiao, G. Jin, B.D. Gates, N.R. Branda, Angew. Chem. Int. Ed. 48 (2009) 4166.
[23] Sh. Yamashita, H. Fukushima, Y. Niidome, T. Mori, Y. Katayama, T. Niidome, Langmuir 27 (2011) 14621.
[24] M.A. Asadirad, N.R. Branda, J. Am. Chem. Soc. 137 (8) (2015) 2824.
[25] N. Abadeer, C.J. Murphy, J. Phys. Chem. C 120 (2016) 4691.
[26] F. Morales-Zavala, H. Arriagada, N. Hassan, C. Velasco, A. Riveros, A.R. Álvarez, A.N. Minniti, X. Rojas-Silva, L.L. Muñoz, R. Vasquez, K. Rodriguez, K. Rodriguez, M. Sanchez-Navarro, E. Giralt, E. Araya, R. Aldunate, M.J. Kogan, Nanomed. Nanotechnol. Biol. Med. 13 (7) (2017) 2341.
[27] C. Adura, S. Guerrero, E. Salas, L. Medel, A. Riveros, J. Mena, J. ArbioL, F. Albericio, E. Giralt, M.J. Kogan, ACS Appl. Mater. Interfaces 5 (10) (2013) 4076.
[28] R. Prades, S. Guerrero, E. Araya, C. Molina, E. Salas, E. Zurita, J. Selva, G. Egea, C. López-Iglesias, M. Teixidó, M.J. Kogan, E. Giralt, Biomaterials 33 (29) (2012) 7194.
[29] H. Hinterwirth, S. Kappel, T. Waitz, T. Prohaska, W. Lindner, M. Lämmerhofer, ACS Nano 7 (2) (2013) 1129.
[30] R.F. Aroca, R.A. Alvarez-Puebla, N. Pieczonka, S. Sanchez-Cortez, J.V. Garcia-Ramos, Adv. Colloid Interface Sci. 116 (2005) 45–61.
[31] E.J. Blackie, E.C. Le Rum y, P.G. Etchegoin, J. Am. Chem. Soc. 131 (40) (2009) 14466.
[32] K. Kneipp, Y. Wang, H. Kneipp, L.T. Perelman, I. Itzkan, R.R. Dasari, M.S. Feld, Phys. Rev. Lett. 78 (1997) 1667–1670.
[33] A.M. Vera, J.J. Cárcamo, A. Aliaga, J.S. Gómez-Jeria, M.J. Kogan, M.M. Campos-Vallette, Spectrochim. Acta Part A 134 (2015) 251.
[34] D. Lin-Vien, N.B. Colthup, W.G. Fateley, J.G. Graselli, The Handbook of Infrared and Raman Characteristic Frequencies of Organic Molecules, Academic Press Boston, 1991.
[35] G. Socrates, Infrared and Raman Characteristic Group Frequencies, Tables and Charts, John Wiley & Sons, Chichester, 2001.
[36] M. Moskovits, Rev. Mod. Phys. 57 (1985) 783.
[37] R. Aroca, Surface-enhanced Vibrational Spectroscopy, John Wiley & Sons, Chichester, 2006.
[38] S. Bhana, R. O'Connor, J. Johnson, J.D. Ziebarth, L. Henderson, X.H. Huang, J. Colloid Interface Sci. 469 (2016) 8.